Available online at www.sciencedirect.com
ScienceDirect
European Journal of Mechanics B/Fluids 26 (2007) 344–353

The absolute instability of the boundary layer on a rotating cone

S.J. Garrett [a,*], N. Peake [b]

[a] *Department of Mathematics, University of Leicester, University Road, Leicester, LE1 7RH, UK*
[b] *Department of Applied Mathematics and Theoretical Physics, University of Cambridge, Wilberforce Road, Cambridge CB3 0WA, UK*

Received 13 September 2005; received in revised form 4 April 2006; accepted 17 August 2006

Available online 25 September 2006

Abstract

This paper is concerned with the existence of local absolute instability in the boundary-layer flow over the outer surface of a rotating cone, thereby extending earlier work by Lingwood who considered the rotating disk. Both still outer fluids and non-zero axial flow are considered, viscous and streamline-curvature effects are included, and the analysis is conducted for a wide range of cone half-angles, ψ. In still outer fluid our predicted local Reynolds numbers at the onset of absolute instability is relatively insensitive to the value of ψ, and is in reasonable agreement with experimental data for the onset of turbulence when $\psi > 50°$. For $\psi < 50°$ the discrepancy increases, suggesting that some other mechanism may be responsible for transition on more slender cones. The introduction of axial flow is found to significantly increase the Reynolds number for local absolute instability for each half-angle.

Keywords: Boundary layer; Absolute instability; Rotating cone

1. Introduction

There has been considerable recent interest in the role of absolute instability in the transition to turbulence on a rotating disk, following the important discovery by Lingwood [1,2] of the presence of absolute instability for local Reynolds numbers in excess of a value very close to the experimentally measured transition location. Lingwood's analysis has been extended to the case of a rotating sphere by the present authors, both in still fluid, [3], and in uniform axial flow [4]. The aim of the current paper is to investigate the existence of local absolute instability on an axisymmetric rotating cone of general half-angle ψ, in both still fluid and axial flow. The case of still outer fluid with $\psi = 90°$ then corresponds to Lingwood's calculations.

The transition of the boundary layer on the surface of rotating cones has been the subject of several experimental investigations. Early experimental work was limited to measurements of the transitional Reynolds numbers – see for instance [5–8]. Further to this, detailed flow visualisation and hot-wire measurements by Kobayashi and Izumi [9]; Kobayashi, Kohama and Kurosawa [10] and Kohama [11] demonstrated the existence of spiral vortices in the non-turbulent part of the boundary layer, which are fixed on the cone for all rotation and axial flow rates and which are

* Corresponding author.
E-mail address: s.garrett@mcs.le.ac.uk (S.J. Garrett).

0997-7546/$ – see front matter
doi:10.1016/j.euromechflu.2006.08.002

similar to those observed by Gregory, Stuart and Walker [12] on the rotating disk and Kohama and Kobayashi [13] on the rotating sphere.

Turning to theoretical work on linear stability theory, Kobayashi and Izumi [9] predict the onset of convective instability and associate this with the appearance of the spiral vortices. The predicted critical Reynolds numbers and vortex angles are in close agreement with their experimental values. Similarly, Kobayashi [14] predicts the onset of spiral vortices in the boundary layer of a cone with $\psi = 15°$ rotating in a uniform axial flow, which are consistent with the measurements in [8,13]. The convective instability in the rotating-cone boundary layer is therefore well understood, and in this paper we aim to show that further insight can be gained from linear stability theory, but now looking for absolute instability. In Section 2 the solution of the steady boundary-layer equations is described and the unsteady perturbation equations for the system derived. The absolute instability analyses are conducted in Sections 3.1 and 3.2 for the still outer fluid and non-zero axial flow cases respectively.

2. Formulation

Consider a rigid cone with circular cross-section and half-angle ψ. We choose the fixed orthogonal curvilinear coordinate system $(x^\star, \theta, z^\star)$, as shown in Fig. 1 (stars indicate dimensional quantities), with the origin located at the apex of the cone. The local cross-sectional radius of the cone is $r_\circ^\star = x^\star \sin\psi$. The cone rotates with a constant angular frequency $\Omega^\star$ about its axis of symmetry, and is immersed in a steady flow which is aligned parallel to the axis of symmetry at upstream infinity.

At the edge of the cone boundary layer the dimensional surface velocity distribution (i.e. the slip velocity) along the cone, $U_\circ^\star(x^\star)$, is given by the well-known potential-flow solution discussed by, for instance, Rosenhead [15] and Evans [16]. It takes the power-law form

$$U_\circ^\star(x^\star) = C^\star x^{\star m}.$$

The value of m is related to the cone half-angle (for instance, $m = 1$ when $\psi = 90°$ and $m = 0.1$ when $\psi = 27.72°$), while $C^\star$ is a scale factor determined by the free-stream axial flow incident on the rotating cone. This inviscid solution is a good representation of the real slip velocity, since the separated boundary layer from the cone will tend to run parallel to the cone surface.

The steady velocities are non-dimensionalised using the local surface velocity, $x^\star\Omega^\star \sin\psi$, as

$$U(\eta;\psi) = \frac{U^\star}{x^\star\Omega^\star\sin\psi}, \quad V(\eta;\psi) = \frac{V^\star}{x^\star\Omega^\star\sin\psi}, \quad W(\eta;\psi) = \frac{W^\star}{(\nu^\star\Omega^\star)^{1/2}}, \tag{1}$$

where U, V and W are the non-dimensional velocities in the $x^\star$-, θ- and $z^\star$-directions respectively and $\eta = z^\star(\Omega^\star/\nu^\star)^{1/2}$ is the non-dimensional distance from the cone surface in the normal direction. Note that η is scaled on the boundary-layer thickness $\delta^\star = (\nu^\star/\Omega^\star)^{1/2}$.

The equations that govern the mean flow in the boundary layer are stated by Mangler [17], and are non-dimensionalised using (1) as

$$WU' + \left(U^2 - V^2\right)\sin\psi = mT_s^2\sin\psi + U'', \tag{2}$$

$$WV' + 2UV\sin\psi = V'', \tag{3}$$

$$W' + 2U\sin\psi = 0, \tag{4}$$

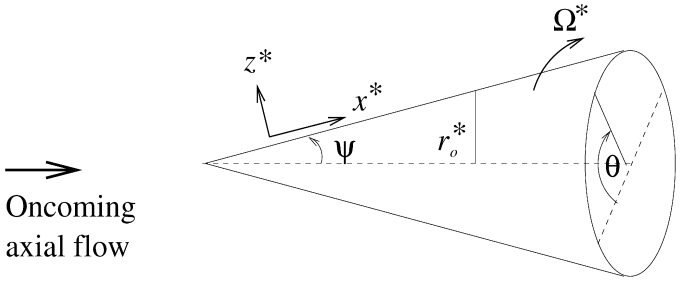

Fig. 1. Sketch of the coordinate system. The angle θ is measured relative to a direction which is fixed in space.

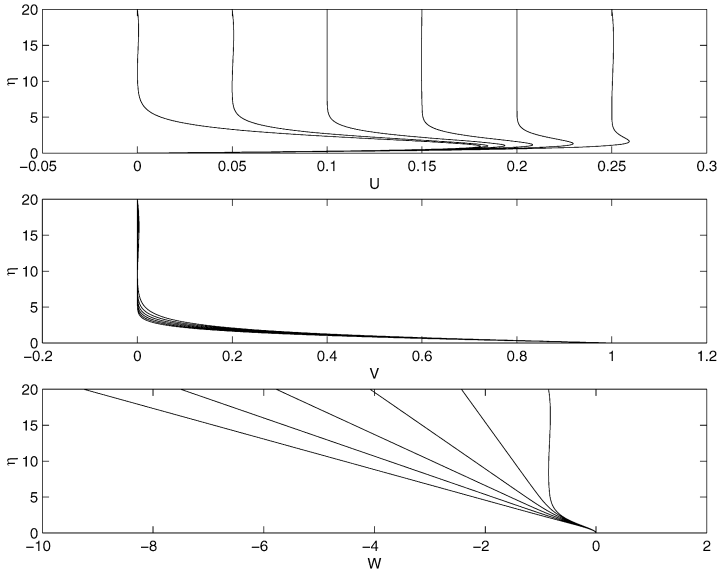

Fig. 2. The steady mean flow velocity profiles for $\psi = 70°$ with $T_s = 0.00$–0.25 in 0.05 increments. For U, increasing T_s moves the profiles left to right; for V and W, right to left.

where a prime denotes differentiation with respect to η. The local axial flow parameter T_s is defined as

$$T_s = \frac{C^\star x^{\star m}}{x^\star \Omega^\star \sin\psi},$$

and is the ratio of the local slip velocity at $x^\star$ to the rotational speed of the cone surface at that location. The non-dimensional boundary conditions are

$$\begin{aligned} &U = W = V - 1 = 0 \quad \text{on } \eta = 0, \\ &V = U - T_s = 0 \quad \text{as } \eta \to \infty, \end{aligned} \tag{5}$$

representing the no-slip condition on the cone surface and the external fluid condition away from the cone respectively.

The choice of scalings will lead to T_s appearing in the mean flow equations only. As we will see, the unsteady perturbation equations are independent of T_s and the effect of non-zero axial flow is simply to change the steady flow profiles upon which the stability analyses are performed, in much the same way as was done in [4] for the rotating-sphere boundary layer in axial flow. However, it is important to note the distinction between the axial flow parameter used in the rotating sphere analysis and the *local* axial flow parameter used here. The fact that T_s depends on both the cone angle ψ and the upstream flow scale factor C^* means that care must be taken in the interpretation of the results of the stability analyses, and this will be discussed later.

The system of Eqs. (2)–(5) are solved numerically for each ψ and T_s using a fourth-order Runge–Kutta integrator with a Newton–Raphson searching routine. Fig. 2 shows the three components of the steady mean flow on a rotating cone with half-angle of $\psi = 70°$ for a range of T_s. We note that the behaviour of the wall-normal velocity profile is similar to that observed in [4] for the rotating sphere in axial flow, i.e. we see W tending to a constant gradient as $\eta \to \infty$ for non-zero T_s. The gradient increases with T_s, and can be calculated from (4) using the second condition of (5) as

$$\frac{\partial W}{\partial \eta} \sim -2T_s \sin\psi.$$

Fig. 2 also shows that the flow very close to the cone surface is independent of the local axial flow parameter.

Absolute instability is a *local* concept, and any analysis requires the impulse response of the system to be determined within the parallel-flow approximation at each streamwise point ($x^* = x_s^\star$) along the surface of the cone. To conduct a local stability analysis at a location $x^* = x_s^\star$ we impose infinitesimally small disturbances on the steady mean flow at that point. We use the non-dimensionalizing length, velocity, pressure and time scales $\delta^\star$, $r_{\circ,s}^\star \Omega^\star$, $\rho^\star r_{\circ,s}^{\star 2} \Omega^{\star 2}$

and $\delta^\star/\Omega^\star r^\star_{\circ,s}$ respectively, where $r^*_{\circ,s}$ is the local radius of cross-section. This leads to the local Reynolds number R at $x^\star_s$, where

$$R = \frac{x^\star_s \Omega^\star \delta^\star \sin\psi}{\nu^\star} = \frac{x^\star_s \sin\psi}{\delta^\star} = x_s \sin\psi = r_{\circ,s},$$

with unstarred quantities being non-dimensional. The instantaneous non-dimensional velocities and pressure are given by

$$\overline{U}(\eta, x, \theta, t; R, \psi) = \frac{r_\circ}{R} U(\eta; \psi) + \hat{u}(\eta, x, \theta, t; R, \psi), \tag{6}$$

$$\overline{V}(\eta, x, \theta, t; R, \psi) = \frac{r_\circ}{R} V(\eta; \psi) + \hat{v}(\eta, x, \theta, t; R, \psi), \tag{7}$$

$$\overline{W}(\eta, x, \theta, t; R, \psi) = \frac{1}{R} W(\eta; \psi) + \hat{w}(\eta, x, \theta, t; R, \psi), \tag{8}$$

$$\overline{P}(\eta, x, \theta, t; R, \psi) = \frac{1}{R^2} P(\eta; \psi) + \hat{p}(\eta, x, \theta, t; R, \psi), \tag{9}$$

where $\hat{u}$, $\hat{v}$, $\hat{w}$ and $\hat{p}$ are the small unsteady perturbations. The non-dimensional continuity and Navier–Stokes equations for the cone geometry are linearised with respect to the perturbation quantities.

In applying the parallel-flow approximation we ignore variation in the local Reynolds number R with local surface cross-sectional radius and assume that $\eta/r_\circ \ll 1$. This involves replacing the variable $r_\circ + \eta\cos\psi$, which appears in the coefficients of the perturbation equations, by R. The resulting stability results are then strictly local, with location $R = r_{\circ,s}$ appearing as a parameter. The assumption $R \gg 1$ (equivalent to $\delta^\star \ll x^\star$) necessarily prohibits analysis close to the apex where $R = \mathrm{O}(1)$. The implications of these approximations are discussed in Section 4.

The perturbation pressure can then be expressed in normal-mode form $\hat{p} = p(\eta;\psi)\exp(\mathrm{i}(\alpha x\sin\psi + \beta\theta - \gamma t))$, with similar expressions for the unsteady velocity. The wavenumber in the x-direction, α, and the frequency, γ, are in general complex, as required by the spatio-temporal analyses conducted later. In contrast, in order to enforce periodicity round the cone the circumferential wavenumber, β, must be interpreted at integer values only. It is assumed that β is $\mathrm{O}(R)$.

The perturbation equations may be written as a set of six first-order ordinary-differential equations using the transformed variables

$$\phi_1 = (\bar{\alpha} - \mathrm{i}\sin\psi/R)u + \bar{\beta}v, \quad \phi_2 = (\bar{\alpha} - \mathrm{i}\sin\psi/R)u' + \bar{\beta}v', \quad \phi_3 = w,$$
$$\phi_4 = p, \quad \phi_5 = (\bar{\alpha} - \mathrm{i}\sin\psi/R)v + \bar{\beta}u, \quad \phi_6 = (\bar{\alpha} - \mathrm{i}\sin\psi/R)v' + \bar{\beta}u',$$

where $\bar{\alpha} = \alpha\sin\psi$, $\bar{\beta} = \beta/R$ and the prime denotes differentiation with respect to η. These equations are

$$\phi_1' = \phi_2, \tag{10}$$

$$\left[\frac{\phi_2'}{R}\right]_v = \frac{1}{R}\left(\left[\bar{\alpha}^2 + \bar{\beta}^2\right]_v + \mathrm{i}R(\bar{\alpha}U + \bar{\beta}V - \gamma) + [U\sin\psi]_s\right)\phi_1 + \left[\frac{W\phi_2}{R}\right]_s + \left(\left(\bar{\alpha} - \left[\frac{\mathrm{i}\sin\psi}{R}\right]_s\right)U' + \bar{\beta}V'\right)\phi_3 + \mathrm{i}\left(\bar{\alpha}^2 + \bar{\beta}^2 - \left[\frac{\mathrm{i}\bar{\alpha}}{R}\right]_s\right)\phi_4 - \left[\frac{2V\sin\psi\phi_5}{R}\right]_s, \tag{11}$$

$$\phi_3' = -\mathrm{i}\phi_1 - \left[\frac{\phi_3\cos\psi}{R}\right]_s, \tag{12}$$

$$\phi_4' = \left[\frac{\mathrm{i}W\phi_1}{R}\right]_s - \left[\frac{\mathrm{i}\phi_2}{R}\right]_v - \frac{1}{R}\left(\left[\bar{\alpha}^2 + \bar{\beta}^2\right]_v + \mathrm{i}R(\bar{\alpha}U + \bar{\beta}V - \gamma) + W_s'\right)\phi_3, \tag{13}$$

$$\phi_5' = \phi_6, \tag{14}$$

$$\left[\frac{\phi_6'}{R}\right]_v = \left[\frac{2V\sin\psi\phi_1}{R}\right]_s + \left(\left(\bar{\alpha} - \left[\frac{\mathrm{i}\sin\psi}{R}\right]_s\right)V' - \bar{\beta}U'\right)\phi_3 + \frac{1}{R}\left(\left[\bar{\alpha}^2 + \bar{\beta}^2\right]_v + \mathrm{i}R(\bar{\alpha}U + \bar{\beta}V - \gamma) + [U\sin\psi]_s\right)\phi_5 + \left[\frac{\bar{\beta}\sin\psi\phi_4}{R}\right]_s + \left[\frac{W\phi_6}{R}\right]_s, \tag{15}$$

where the subscripts v and s indicate which of the $O(R^{-1})$ terms arise from the viscous and streamline-curvature effects respectively.

With $\psi = 90°$, (10)–(15) reduce to the perturbation equations relevant to rotating-disk boundary layer. It should be noted, however, that these are slightly different to those used by Lingwood who formulates the problem in a rotating frame of reference. The use of a rotating frame naturally leads to Coriolis terms that do not appear in (10)–(15); we will see that this leads to a different definition of γ_r.

The streamline-curvature terms (which appear here and in Lingwood's formulation) represent the effect of deflection of the inviscid-flow streamlines through the action of the pressure gradient. By neglecting these terms in (10)–(15), the system of equations reduces to the Orr–Sommerfeld equation for the rotating cone in the form

$$\frac{\mathrm{i}}{R}\left(\phi_3'''' - 2\left(\bar{\alpha}^2+\bar{\beta}^2\right)\phi_3'' + \left(\bar{\alpha}^2+\bar{\beta}^2\right)^2\phi_3\right) + (\bar{\alpha}U + \bar{\beta}V - \gamma)\left(\phi_3'' - \left(\bar{\alpha}^2+\bar{\beta}^2\right)\phi_3\right) - \left(\bar{\alpha}U'' + \bar{\beta}V''\right)\phi_3 = 0. \tag{16}$$

Neglecting both the streamline-curvature and viscous terms in the perturbation equations leads to Rayleigh's equation in the form

$$(\bar{\alpha}U + \bar{\beta}V - \gamma)\left(\phi_3'' - \left(\bar{\alpha}^2+\bar{\beta}^2\right)\phi_3\right) - \left(\bar{\alpha}U'' + \bar{\beta}V''\right)\phi_3 = 0. \tag{17}$$

3. Absolute instability analysis

We now proceed to investigate the possible existence of local absolute instability in the cone boundary layer. This involves solution of the eigenvalue problem defined by (10)–(15), with the homogeneous boundary conditions, at each Reynolds number, R, to form the dispersion relation $D(\alpha, \beta, \gamma; R, \psi) = 0$. Details of the numerical procedure are given in [3].

We use the Briggs–Bers criterion [18,19] to detect absolutely unstable behaviour in the long-time response to an initial perturbation of the form $\delta(r - r_s)\delta(t)\mathrm{e}^{\mathrm{i}\beta\theta}$. For absolute instability to occur we need to locate a pinch point $(\alpha^\circ, \gamma^\circ)$, formed by coalescence between two spatial branches which originated from distinct half-α-planes when γ_i is sufficiently large and positive. The flow is then absolutely unstable if $\gamma_i > 0$ at the pinch point, and is otherwise at worst convectively unstable. We will see that a pinch point can indeed be found for each cone angle ψ and flow parameter T_s, which is unstable for sufficiently large R. By monitoring the behaviour of these two spatial branches as the Reynolds number is varied, it is possible to determine the critical value of R for the onset of absolute instability to the required degree of accuracy. We present the critical Reynolds numbers here to two decimal places.

As with the rotating disk [1] and rotating sphere [3,4], analysis of the Orr–Sommerfeld equation (16) (at very high Reynolds number) and the Rayleigh equation (17) demonstrate that the pinch is formed by the coalescence of two modes which are inviscid in origin. For this reason we present only an analysis of the full perturbation equations (10)–(15) here, but note that the pinch arises between modes often referred to as "type 1" and "type 3" in the literature. Further details can be found in [20].

3.1. Cone rotating in still fluid, $T_s = 0$

We begin by studying the cone rotating in *still* fluid, i.e. $T_s = 0$. Pinch points with $\gamma^\circ > 0$ have been found for all cone half-angles, and so the boundary layer on each cone is absolutely unstable for certain values of R and β. Fig. 3 shows the neutral stability curves for absolute instability in the (R, γ_r°)-, (R, α_r°)-, (R, α_i°)- and (R, β)-planes, the flow being absolutely unstable inside each curve. The figure shows that the onset of absolute instability occurs at a lower Reynolds number for the more slender cones which, for a fixed rotation rate, corresponds to a smaller local cross-sectional radius. However, an alternative measure of the position of onset of the absolute instability is the non-dimensional distance along the cone surface from the tip, $x = R/\sin\psi$, and the critical values of R and x at the onset of absolute instability are shown in Table 1 for each cone. We see that for a given rotation rate the onset of absolute instability occurs further along the more slender cones. The result for $\psi = 90°$ in Table 1 agrees with Lingwood's [1] value for the rotating disk (as corrected in [21]). Critical values for γ_r°, α° and $\bar{\beta}$ at the onset of absolute instability are given in Appendix A for each ψ. We note that for $\psi = 90°$ (and $T_s = 0$) the critical values of α° and $\bar{\beta}$ also agree with Lingwood's results. The value of γ_r° differs, but this is due to the different frames of reference used.

Table 1
The critical values of R, x and R_X for the onset of absolute instability for each cone

ψ	$r = R$	$x = R/\sin\psi$	R_X
15	249.63	964.50	2.408×10^5
20	289.95	847.76	2.458×10^5
30	353.47	706.94	2.499×10^5
40	402.49	626.16	2.520×10^5
50	440.60	575.16	2.534×10^5
60	469.42	542.04	2.544×10^5
70	489.78	521.21	2.553×10^5
80	502.12	509.87	2.560×10^5
90	507.32	507.32	2.574×10^5

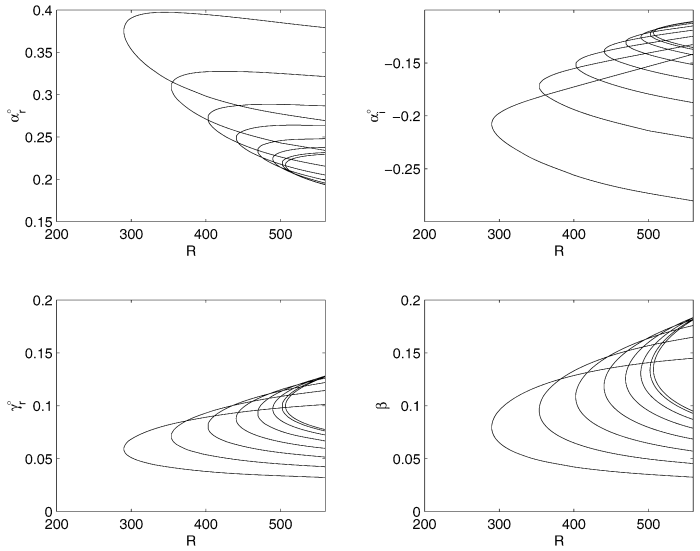

Fig. 3. Absolute instability neutral curves in the (R, α_r^o)-, (R, α_i^o)-, (R, γ_r^o)- and $(R, \bar{\beta})$-planes for cones with half-angles of $\psi = 20°$–$90°$ in $10°$ increments (left to right).

Fig. 4 shows a comparison between the predicted onset of absolute instability and experimentally measured transition points of Kobayashi and Izumi [9], using the local Reynolds number $R_X = x^{\star 2}\Omega^\star \sin\psi/\nu^\star = R^2/\sin\psi$ for each half-angle.

For cone half-angles above $\psi = 50°$ the experimental results show that transition occurs at roughly the same local Reynolds number for each cone half-angle, despite the instability waves first appearing across a wide parameter range with varying rotation rate. This experimental observation leads us to expect that the underlying transition mechanism here is an absolute instability, and indeed there is reasonable agreement between the experimental transition location and our predicted absolute-instability boundary for $\psi > 50°$. Note, however, that Kobayashi and Izumi measure a local Reynolds number of 566 for transition on the rotating disk ($\psi = 90°$), which differs from Lingwood's [2] experimental measurement of between $R = 502$ and $R = 514$ (which in turn is itself close to results from a number of other experimental papers, see [1,2] for details). This discrepancy is presumably due to different experimental definitions of transition location. As can be seen, our predicted local Reynolds numbers for the absolute-instability boundary for any ψ are all very close to Lingwood's value for the rotating disk. Below $\psi = 50°$ we see that R_X at the experimental transition point decreases sharply with half-angle, and we hypothesise that this indicates that the underlying transition mechanism in these experiments is no longer absolute instability for the more slender cones.

We have seen in Table 1 and Fig. 4 that the predicted onset of absolute instability occurs at roughly the same local Reynolds number for all cones, $R_X \approx 2.5 \times 10^5$. Interestingly, this is reasonably close to the value calculated for the rotating-sphere boundary layer in still fluid [3], in circumstances in which the onset is close to the pole (latitude

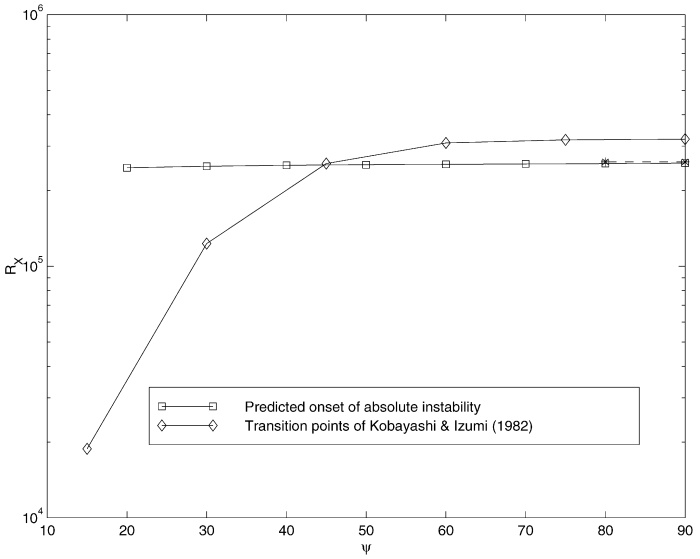

Fig. 4. A comparison of the predicted critical R_X values for the onset of absolute instability with the transitional values measured by Kobayashi and Izumi (1982). The dashed line shows the transition value on the rotating disk as measured by [2].

Table 2
The critical Reynolds numbers R for the onset of absolute instability for half-angles $\psi = 20°$–$90°$ and local axial flow parameters $T_s = 0.00$–0.25

T_s	20°	30°	40°	50°	60°	70°	80°	90°
0.00	249.63	289.95	353.47	402.49	440.60	489.78	502.12	507.32
0.05	339.13	410.94	468.79	516.62	556.37	588.86	614.72	634.23
0.10	394.68	476.92	549.84	617.75	682.99	746.53	810.09	875.18
0.15	461.01	558.18	655.56	758.10	870.13	994.03	1136.17	1304.48
0.20	561.26	661.00	796.18	955.48	1148.74	1385.54	1686.23	2083.31
0.25	684.08	792.92	985.95	1236.77	1570.28	2017.32	2641.24	3956.59

$\theta = 0°$). For instance, if absolute instability first occurs at latitude $\theta = 30°$ on the sphere then the critical local Reynolds number is 2.15×10^5. Of course, this is due to the fact that close to the pole the steady boundary-layer flow on the sphere approximates the disk boundary layer. When the absolute-instability boundary on the sphere is located at higher latitudes, we show in [3] that the critical value of R_X drops quite significantly.

3.2. Cone rotating in uniform axial flow, $T_s \neq 0$

In this subsection we repeat the analysis presented in Section 3.1 but now with non-zero axial flow. Recall that the local axial flow parameter, T_s, is the ratio of the local slip velocity to the local velocity of the body due to rotation, and this means that care must be taken in the interpretation of the results. For instance, moving along a generator of a given cone away from the vertex, at fixed rotation rate, one finds that T_s decreases continuously, even though the slip velocity increases (because the slip-velocity index, m, is less than unity for $\psi < 90°$). Alternatively, if we compare cones of different half angles at fixed rotation rate, then since m depends on ψ it follows that one would have to change the axial flow scale $C^\star$ in order to keep T_s fixed.

Using exactly the same procedure as in the previous subsection, pinch-points with $\gamma_i > 0$ have been found for all half-angles for each value of the local axial flow parameter, and so the boundary layers on cones rotating in a uniform axial flow are absolutely unstable for certain values of R and β for each half-angle. The neutral curves are similar to those shown in Fig. 3 and need not be included. The critical Reynolds numbers for the onset of absolute instability for each half-angle are shown in Table 2 for local axial flow parameters of $T_s = 0.00$–0.25; the critical values of all parameters are given in the appendix. These results show that axial flow stabilises the boundary layer to absolute instabilities for each half-angle, i.e. the critical Reynolds numbers are increased with increased T_s for each ψ.

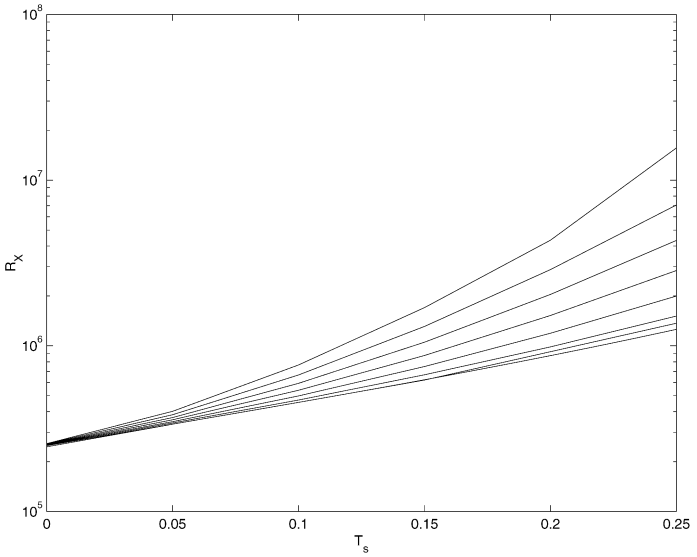

Fig. 5. Predicted critical R_X values for absolute instability against T_s for $\psi = 20°$–$90°$ in $10°$ increments (bottom to top).

For reasons discussed above, the use of the local axial flow parameter, T_s, means that the critical local Reynolds numbers for cones with different half-angles cannot be directly compared for fixed T_s. Instead, in Fig. 5 we plot the critical local Reynolds numbers against T_s for each ψ. This figure shows that increasing T_s increases the critical local Reynolds numbers found for each separate cone half-angle, ψ. Note that as T_s increases away from zero the local critical Reynolds number becomes increasingly sensitive to the value of ψ.

Experiments that measure the onset of turbulence on cones rotating in axial flow have been conducted [8,10] for a half angle of $\psi = 15°$ only. In [10] the measured values of R_X increase as T_s is increased (note that in the notation of [10], $S = 1/T_s$ and $Re_x = T_s R_X$), and this is consistent with our prediction of the behaviour of the absolute instability boundary. However, the transition Reynolds numbers measured in [10] are again significantly lower than our prediction (for instance, with $T_s = 0.2$ from Fig. 6 of [10] we find $R_X \approx 5 \times 10^4$, compared to our prediction of $R_X = 8.88 \times 10^5$). This again suggests that absolute instability may not be causing transition on these slender cones.

4. Concluding remarks

In this paper we have shown that the boundary layer on the outer surface of a rotating cone is locally absolutely unstable, across apparently the whole range of cone angles, and with and without exterior axial flow. In otherwise still outer fluid the local Reynolds number at the absolute instability boundary is relatively insensitive to the cone angle, and for cone half angles in excess of $50°$ is in reasonable agreement with Kobayashi and Izumi's [9] experimentally measured values at the transition location. The introduction of outer flow tends to stabilise the absolute instability, in the sense that as the local flow parameter T_s increases from zero the absolute instability boundary is pushed to larger R_X.

During this analysis we have made use of a parallel-flow approximation by assuming that factors

$$1 + \eta \cos\psi / R, \tag{18}$$

can be replaced by unity. We are careful to point out that this approximation would imply that the resulting perturbation equations are not consistent to $O(R^{-1})$, the same order as the viscous and streamline-curvature terms. Therefore, whether using the Orr–Sommerfeld equation (16) or the full perturbation equations (10)–(15), the solutions cannot be justified rigorously at finite Reynolds number. It is the authors' opinion that this approximation does not affect the conclusions presented here since absolute instability is known to arise from inviscid modes which are observable in the purely inviscid and rigorous analysis of the Rayleigh equation (17). However, we do acknowledge that the numerical results presented may be subject to slight inaccuracies as a result of the approximation. The basic flow is shown in Fig. 2 for $\psi = 70°$ only, but we note that similar profiles were observed at all ψ. From this we see that the

boundary-layer is fully developed when $\eta \approx 10$, and so the quantity $\eta \cos\psi$ reduces to zero as the half-angle tends to 90°. This, together with the observation that critical Reynolds numbers increase with ψ and T_s, imply that the parallel-flow approximation is less valid for slender cones rotating in an otherwise still fluid. We can quantify the inaccuracy by noting that $R \approx 290$ at the onset of absolute instability for $\psi = 20°$ and $T_s = 0$, which means that factor (18) is approximated by unity with an inaccuracy of less than 4%.

The results of this paper are restricted to local linear stability. The question of the global-linear stability of the rotating disk has been investigated by Davies and Carpenter [22], who show that the global mode associated with the local absolute instability is damped. Given the close relationship between the boundary layers on rotating disks and rotating cones, one may also expect this to hold for the rotating cone (at least for large half angle). Note, however, that this does not imply that absolute instability is not involved in transition. Pierre and Huerre [23] have shown that when non-linear effects are included a self-sustained non-linear oscillator will always be generated when there is a region of local linear absolute instability. On the rotating disk, Pier [24] has shown that this oscillator will undergo secondary instability close to the absolute instability boundary, providing a possible route to transition. The global behaviour needs to be investigated for the cone boundary layer, perhaps with a view to understanding the apparent change in behaviour when the cone angle is reduced.

Acknowledgements

This work was supported by the Engineering and Physical Sciences Research Council and the Newton Trust of Cambridge University.

Appendix A. Critical values for the onset of absolute instability

Table 3

$\psi = 90°$					$\psi = 80°$				
T_s	R	$\gamma°$	$\alpha°$	$\bar{\beta}°$	T_s	R	$\gamma°$	$\alpha°$	$\bar{\beta}°$
0.00	507.32	0.099	0.217 − i0.122	0.135	0.00	502.12	0.099	0.219 − i0.122	0.134
0.05	634.23	0.117	0.209 − i0.133	0.158	0.05	614.71	0.114	0.212 − i0.133	0.155
0.10	875.18	0.132	0.195 − i0.143	0.178	0.10	810.09	0.129	0.200 − i0.143	0.173
0.15	1304.48	0.145	0.177 − i0.150	0.192	0.15	1136.17	0.141	0.184 − i0.150	0.187
0.20	2083.31	0.154	0.158 − i0.154	0.199	0.20	1686.23	0.151	0.168 − i0.155	0.197
0.25	3956.59	0.164	0.129 − i0.155	0.208	0.25	2641.24	0.156	0.151 − i0.156	0.200
$\psi = 70°$					$\psi = 60°$				
T_s	R	$\gamma°$	$\alpha°$	$\bar{\beta}°$	T_s	R	$\gamma°$	$\alpha°$	$\bar{\beta}°$
0.00	489.78	0.097	0.224 − i0.125	0.131	0.00	469.42	0.093	0.234 − i0.131	0.126
0.05	588.86	0.111	0.218 − i0.136	0.150	0.05	556.36	0.106	0.228 − i0.141	0.143
0.10	746.53	0.124	0.208 − i0.145	0.167	0.10	682.99	0.117	0.219 − i0.150	0.158
0.15	994.03	0.135	0.195 − i0.153	0.180	0.15	870.13	0.127	0.208 − i0.158	0.170
0.20	1385.54	0.144	0.180 − i0.158	0.189	0.20	1148.74	0.136	0.195 − i0.164	0.180
0.25	2017.31	0.151	0.165 − i0.161	0.195	0.25	1570.28	0.143	0.182 − i0.168	0.186
$\psi = 50°$					$\psi = 40°$				
T_s	R	$\gamma°$	$\alpha°$	$\bar{\beta}°$	T_s	R	$\gamma°$	$\alpha°$	$\bar{\beta}°$
0.00	440.60	0.088	0.249 − i0.139	0.118	0.00	402.49	0.081	0.272 − i0.152	0.109
0.05	516.61	0.099	0.244 − i0.150	0.134	0.05	468.79	0.091	0.267 − i0.163	0.122
0.10	617.75	0.109	0.236 − i0.159	0.147	0.10	549.84	0.099	0.260 − i0.173	0.133
0.15	758.10	0.118	0.226 − i0.167	0.158	0.15	655.56	0.106	0.252 − i0.182	0.143
0.20	955.48	0.125	0.215 − i0.174	0.166	0.20	796.18	0.113	0.242 − i0.189	0.151
0.25	1236.77	0.132	0.204 − i0.179	0.173	0.25	985.95	0.119	0.232 − i0.195	0.157
$\psi = 30°$					$\psi = 20°$				
T_s	R	$\gamma°$	$\alpha°$	$\bar{\beta}°$	T_s	R	$\gamma°$	$\alpha°$	$\bar{\beta}°$
0.00	353.47	0.071	0.309 − i0.172	0.096	0.00	289.95	0.059	0.375 − i0.208	0.080
0.05	410.94	0.080	0.304 − i0.186	0.108	0.05	339.13	0.067	0.370 − i0.226	0.091
0.10	476.92	0.087	0.297 − i0.197	0.118	0.10	394.68	0.073	0.363 − i0.241	0.099
0.15	558.18	0.094	0.290 − i0.207	0.126	0.15	461.01	0.079	0.355 − i0.254	0.106
0.20	661.00	0.099	0.282 − i0.215	0.133	0.20	561.26	0.082	0.344 − i0.269	0.111
0.25	792.92	0.104	0.273 − i0.223	0.138	0.25	684.08	0.084	0.329 − i0.281	0.115

References

[1] R.J. Lingwood, Absolute instability of the boundary layer on a rotating disk, J. Fluid Mech. 299 (1995) 17–33.
[2] R.J. Lingwood, An experimental study of absolute instability of the rotating-disk boundary-layer flow, J. Fluid Mech. 314 (1996) 373–405.
[3] S.J. Garrett, N. Peake, The stability and transition of the boundary layer on a rotating sphere, J. Fluid Mech. 456 (2002) 199–217.
[4] S.J. Garrett, N. Peake, The stability of the boundary layer on a rotating sphere in a uniform axial flow, Eur. J. Mech. B 23 (2004) 241–253.
[5] F. Kreith, D. Ellis, J. Giesing, An experimental investigation of the flow engendered by a rotating cone, Appl. Sci. Res. A 11 (1962) 430–440.
[6] C.L. Tein, D.T. Campbell, Heat and mass transfer from rotating cones, J. Fluid Mech. 17 (1963) 105–112.
[7] R. Kappesser, R. Greif, I. Cornet, Mass transfer on rotating cones, Appl. Sci. Res. 28 (1973) 442–452.
[8] F. Salzberg, S.P. Kezios, Mass transfer from a rotating cone in axisymmetric flow, J. Heat Transfer 87 (1965) 469–476.
[9] R. Kobayashi, H. Izumi, Boundary-layer transition on a rotating cone in still fluid, J. Fluid Mech. 127 (1983) 353–364.
[10] R. Kobayashi, Y. Kohama, M. Kurosawa, Boundary-layer transition on a rotating cone in axial flow, J. Fluid Mech. 127 (1983) 341–352.
[11] Y. Kohama, Behaviour of spiral vortices on a rotating cone in axial flow, Acta Mech. 51 (1984) 105–117.
[12] N. Gregory, J.T. Stuart, W.S. Walker, On the stability of three-dimensional boundary layers with application to the flow due to a rotating disk, Philos. Trans. R. Soc. Lond. Ser. A 248 (1955) 155–199.
[13] Y. Kohama, R. Kobayashi, Boundary-layer transition and the behaviour of spiral vortices on rotating spheres, J. Fluid Mech. 137 (1983) 153–164.
[14] R. Kobayashi, Linear stability theory of boundary layer along a cone rotating in axial flow, Bull. Japan Soc. Mech. Engrs. 24 (1981) 934–940.
[15] L. Rosenhead, Laminar Boundary Layers, Oxford University Press, Oxford, 1963.
[16] H. Evans, Laminar Boundary Layer Theory, Addison-Wesley, 1968.
[17] W. Mangler, Boundary layers on bodies of revolution in symmetrical flow, Ber. Aerodyn Versuchsanst. Goett., Report 45/A/17, 1945.
[18] R.J. Briggs, Electron-Stream Interaction with Plasmas, MIT Press, 1964 (Chapter 2).
[19] A. Bers, Linear waves and instabilities, in: C. DeWitt, J. Peyraud (Eds.), Physique des Plasmas, Gordon & Breach, 1975 (Chapter 4).
[20] S.J. Garrett, The stability and transition of the boundary layer on rotating bodies, PhD thesis, Cambridge University, 2002.
[21] R.J. Lingwood, Absolute instability of the Ekman layer and related rotating flows, J. Fluid Mech. 331 (1997) 405–428.
[22] C. Davies, P.W. Carpenter, Global behaviour corresponding to the absolute instability of the rotating-disk boundary layer, J. Fluid Mech. 486 (2003) 287–329.
[23] B. Pier, P. Huerre, Nonlinear self-sustained structures and fronts in spatially developing wake flows, J. Fluid Mech. 435 (2001) 359–381.
[24] B. Pier, Finite-amplitude crossflow vortices, secondary instability and transition in the rotating-disk boundary layer, J. Fluid Mech. 487 (2003) 315–343.